

Dynamics of large-scale solar-wind streams obtained by the double superposed epoch analysis. 2. CIR.vs.Sheath and MC.vs.Ejecta comparisons

Yu. I. Yermolaev,¹ I. G. Lodkina,¹ N. S. Nikolaeva,¹ M. Yu. Yermolaev¹

arXiv:1602.08899v1 [physics.space-ph] 29 Feb 2016

¹Space Plasma Physics Department,
Space Research Institute, Russian Academy
of Sciences, Profsoyuznaya 84/32, Moscow
117997, Russia. (yermol@iki.rssi.ru)

Abstract.

This work is a continuation of our previous paper [*Yermolaev et al.*, 2015] which describes the average temporal profiles of interplanetary plasma and field parameters in large-scale solar-wind (SW) streams: CIR, ICME (both MC and Ejecta) and Sheath as well as the interplanetary shock (IS). Like in the previous work we use data of OMNI database, our catalog of large-scale solar-wind phenomena during 1976–2000 [*Yermolaev et al.*, 2009a] and the double superposed epoch analysis (DSEA) method [*Yermolaev et al.*, 2010a]: re-scaling the duration of interval for all types in such a manner that, respectively, beginning and end for all intervals of selected type coincide. We present new detailed results of comparison of two pair phenomena: (1) both types of compression regions (CIR.vs.Sheath) and (2) both types of ICMEs (MC.vs.Ejecta). Obtained data allows us to suggest that the formation of all types of compression regions has the same physical mechanism irrespective of piston (High-Speed Stream (HSS) or ICME) type and differences are connected with geometry (angle between speed gradient in front of piston and satellite trajectory) and full jumps of speed in edges of compression regions. One of consequences of this hypothesis is the conclusion that one of the reasons of observed distinctions of parameters in MC and Ejecta can be fact that at measurements of Ejecta the satellite passes further from the nose area of ICME, than at measurements of MC. We also discuss the impact of Sheath in magnetospheric activity and its contribution in estimation of Sun’s open magnetic flux.

1. Introduction

The disturbed types of the solar wind (SW) is one of the key links of space weather chain because only disturbed types of SW streams can contain the interplanetary magnetic field (IMF) component perpendicular to the ecliptic plane (in particular the southward IMF component) and be the main source of magnetospheric disturbances including the magnetic storms [*Russell et al.*, 1974; *Burton et al.*, 1975; *Akasofu*, 1981]. Such disturbed types are the following SW streams: interplanetary manifestation of coronal mass ejection (ICME) including magnetic cloud (MC) and Ejecta, Sheath - compression region before ICME, and corotating interaction region (CIR) - compression region before high-speed stream (HSS) of solar wind (see reviews and recent papers by *Gonzalez et al.* [1999]; *Huttunen and Koskinen* [2004]; *Wimmer-Schweingruber et al.* [2006]; *Zurbuchen and Richardson* [2006]; *Tsurutani et al.* [2006]; *Yermolaev and Yermolaev* [2006, 2010]; *Yermolaev et al.* [2007, 2012]; *Zhang et al.* [2007]; *Jian et al.* [2008]; *Borovsky and Denton* [2010]; *Thatcher and Müller* [2011]; *Richardson and Cane* [2012]; *Mitsakou and Moussas* [2014]; *Hietala et al.* [2014]; *Cid et al.* [2014]; *Wu and Lepping* [2015]; *Katus et al.* [2015]; *Kilpua et al.* [2015]; *Gopalswamy et al.* [2015, 2016] and references therein). To understand geoeffectiveness of various types of SW streams, it is necessary to compare the characteristics of the streams inducing magnetospheric disturbances with the characteristics of all events of this type independently of possibility of disturbance generation. In the present work we analyze full sets of various solar wind types for interval 1976-2000 on the basis of OMNI data.

This paper is a continuation of our recent paper [Yermolaev *et al.*, 2015] in which we studied the average temporal behavior of plasma and field parameters of disturbed SW types by the double superposed epoch analysis (DSEA) method which allows one to investigate phenomena with different durations [Yermolaev *et al.*, 2010a]. To consider the influence of both the surrounding undisturbed SW types and the interaction of the disturbed SW types on the parameters, we separately analyzed the following sequences of the phenomena: (1) SW/CIR/SW, (2) SW/IS/CIR/SW, (3) SW/Ejecta/SW, (4) SW/Sheath/Ejecta/SW, (5) SW/IS/Sheath/Ejecta/SW, (6) SW/MC/SW, (7) SW/Sheath/MC/SW, (8) SW/IS/Sheath/MC/SW, where abbreviation IS means the interplanetary shock. This analysis allowed us to obtain several interesting results. In particular, we showed that the behavior of parameters in Sheath and in CIR are very similar both qualitatively and quantitatively. Both the high-speed stream (HSS) and the fast ICME play a role of pistons which push the plasma located ahead them and result of compression does not depend on type of piston. Besides, we obtained the clear evidence of ICME interaction with surrounding SW.

In present work we continue our analysis and present new detailed results of comparison of two pair phenomena: (1) both types of compression region (CIR.vs.Sheath) and (2) both types of ICME (MC.vs.Ejecta). We also discussed the geoeffectiveness of compression regions and their contribution in the estimation of the Sun's open magnetic flux. The organization of the paper is as follows: Section 2 describes data and method. In Section 3, we present results on CIR.vs.Sheath and MC.vs.Ejecta comparisons. Section 4 discusses and summarizes the results.

2. Methods

The data and methods used in this work are similar to those which have been used in the previous work [*Yermolaev et al.*, 2015]: the 1-h interplanetary plasma and magnetic field data of OMNI database (<http://omniweb.gsfc.nasa.gov> [*King and Papitashvili*, 2004]), our catalog of large-scale solar-wind phenomena during 1976–2000 (<ftp://ftp.iki.rssi.ru/pub/omni/> [*Yermolaev et al.*, 2009a]) and the double superposed epoch analysis (DSEA) method [*Yermolaev et al.*, 2010a]: re-scaling the duration of the interval for all SW types in such a manner that, respectively, beginning and end for all intervals of selected type coincide. We selected only such events for which the SW type and the edges of an interval of the type could be defined on the basis of measurements (measurements of some parameters on this interval could be absent). Numbers of such events were 695 for Ejecta, 451 for CIR, 402 for Sheath, and 60 for MC.

To characterize the value of parameters we use the terms "low", "high" and so forth. These terms are qualitative and are defined by comparison with the average value of the corresponding parameter in the undisturbed solar wind. In order to estimate the existence of temporary change of parameter in selected SW type, we defined the statistical significance of temporal trend as a linear dependence of parameter on time [*Bendat and Piersol*, 1971]. In all cases, when we write about the temporal change, there are linear dependences with probability not less 90%.

3. Results

3.1. Comparison of CIR and Sheath phenomena

Figures 1 and 2 present the average temporal profiles of 22 parameters of plasma and IMF for CIR (green lines), Sheath before Ejecta (blue lines) and Sheath before MC (red

lines) obtained by the double superposed epoch analysis method. Data for phenomena with IS and without IS are shown by thick and thin lines, respectively.

1. The bulk velocity V (Fig.1e).

The velocity V increases for all types of solar wind: for phenomena without IS from ~ 350 – 370 up to ~ 430 – 470 km/s (the line for CIR has the highest slope) and for phenomena with IS from ~ 420 – 450 up to ~ 500 – 520 km/s (the slope for all phenomena is similar).

2. The bulk velocity angles: longitude ϕ and latitude θ (Figs.1c, 1d).

The angle ϕ increases from -3 – -2 up to $+2$ degrees for CIR and from -2 up to $+1$ degrees for Sheath before Ejecta and is approximately constant for Sheath before MC. These dependences are similar both for phenomena with IS and without IS. The angle θ is approximately constant for all SW types and probably decreases from $+3$ down to -1 degrees only for Sheath before MC with IS.

3. The density N (Fig.1b).

The density decreases for all phenomena. For CIR and Sheath before Ejecta it falls rather sharply and monotonously, they with IS have higher value at the beginning of interval due to jump at IS but at the end of interval CIR and Sheath before Ejecta both with IS and without IS have similar density. The density for Sheath before MC with IS at the beginning of interval is close to one for CIR and Sheath before Ejecta with IS but it decreases slowly. The density for Sheath before MC without IS at the beginning of interval is close to one for CIR and Sheath before Ejecta without IS, then it increases in the middle of interval and decreases at the end of interval.

4. The proton temperature T_p (Fig.1a).

For all SW types without IS the temperature grows from $5 \cdot 10^4$ K to $10 \cdot 10^4$ K, and for types of streams with IS it abruptly increases right after IS up to $10 \cdot 10^4$ K, and further does not change on the interval.

5. The sound speed V_s (Fig.1g).

The sound speed changes a little throughout the interval, but it is possible to note that it behaves similar to behavior of temperature in the corresponding SW types.

6. The Alfvén speed V_a (Fig.1f).

The Alfvén speed poorly grows for all SW types, and for streams with IS value V_a is a little higher.

7. The thermal pressure P_t (Fig.1h).

The thermal pressure has characteristic features of both temperature and density. At the beginning of interval the thermal pressure for phenomena with IS is one order of magnitude higher than phenomena without IS, then it in types with IS monotonic decreases and in type without IS increases in first half of interval and decrease a little in second half of interval.

8. The ratio of measured and expected temperatures T/T_{exp} (Fig.1i).

The temperature ratio is larger 1 for all phenomena and it higher for phenomena with IS. The ratio for both Sheath types with IS increases at the IS front and then decreases throughout all interval and it has maxima inside interval for other SW types.

9. The ratio of proton thermal and magnetic pressures (β - parameter) (Fig.1j).

For all phenomena the β - parameter is almost constant (in the range 0.5–0.7) throughout interval and decreases only for Sheath before MC with IS.

10. The magnitude of IMF B (Fig.2b).

For all phenomena without IS B is lower than the for phenomena with IS and has maxima (~ 8 nT for CIR and Sheath before Ejecta and ~ 12 for Sheath before MC) in the middle of interval. For CIR and Sheath before Ejecta with IS B decreases from 12 down to 8 nT, and for Sheath before MC with IS it increases from 10 up to 14 nT.

11. The x-, y- and z-components of IMF (B_x , B_y and B_z) (Fig.2c,d,e).

For all phenomena the average values of B_x , B_y and B_z have small magnitude, are almost constant throughout all interval and change in the region of $-2 - +2$ nT.

12. The y-component of interplanetary electric field $E_y = V_x B_z$ (Fig.2f).

For all phenomena the average value of E_y has small magnitude, is almost constant throughout all interval and change in the region of $-1 - +1$ mV/m.

13. The sound Mach number M_s (Fig.2a).

For all phenomena M_s is almost constant in the region of 7–8 in first half interval and slightly increases in second part of interval.

14. The Alfvén Mach number M_a (Fig.2g).

For all phenomena M_a slightly decreases from 10–12 down to 7–8 and it is almost constant ~ 8 for Sheath before Ejecta with IS.

15. The dynamic pressure P_d (Fig.2h).

For all phenomena with IS P_d is higher than phenomena without IS. For CIR and Sheath before Ejecta with IS P_d decreases from 7 down to 4 dyn, for they without IS it is almost constant ~ 4 . For Sheath before MC without IS it increases from 3 up to 6 in first half of interval and does not change in second half of interval. For Sheath before MC with IS P_d increases from 6 up to 8 dyn.

16. The magnetospheric AE , K_p , D_{st} and D_{st}^* indices (Fig.2i,j,k,l).

Behavior of all indices shows that magnetospheric activity increases throughout all interval. The activity is higher for phenomena with IS than phenomena without IS and activity for CIR is less than for all types of Sheath.

3.2. Magnetic field in CIR and Sheath phenomena

The theoretical estimates of possible magnitudes of magnetic field in compression regions CIR and Sheath and their geoeffectiveness are discussed in the literature (see papers by *Gopalswamy et al.* [2015, 2016] and references therein). These estimates can be compared with results of measurements. Figure 3 presents the dependence of the average and maximal values of magnetic field $\langle B \rangle$ and B_{max} (left and right panels, respectively) on speed of corresponding piston: on the speed of high-speed stream V_{HSS} for CIR (green), on the velocity of Ejecta for Sheath before Ejecta V_{Ej} (blue) and on the velocity of MC for Sheath before MC V_{MC} (red). Straight lines are results of linear approximation of the corresponding data. Thick lines and circles correspond to events with IS, thin lines and crosses to events without IS. Figure 4 has the same structure as figure 3, but unlike figure 3 it represents the average and maximum values of magnetic field related to the values of undisturbed magnetic field before compression region $\langle B \rangle / B_{SW}$ and B_{max} / B_{SW} .

Figure 3 shows that the average and maximal values of magnetic field $\langle B \rangle$ and B_{max} in all types of compression regions increase with increasing velocity of corresponding piston and can reach large values at high velocities of pistons. Though dependence of relative values $\langle B \rangle / B_{SW}$ and B_{max} / B_{SW} on speed of pistons is not observed, figure 4 shows that there are many cases when the average and maximal values of field in compression regions can exceed the field in undisturbed streams more than 4 times: 8 and 33 cases from 553 events for the average and maximal values of field, respectively.

Two examples of such events of 18-21 December 1980 (SW/IS/Sheath/MC/SW phenomena consequence) and 24-27 April 1979 (SW/IS/Sheath/Ejecta/SW consequence) are presented in figures 5 and 6 which have similar structure and show the following parameters: (panel a) the ratio of thermal and magnetic pressures (β - parameter), the thermal pressure P_t , the ratio of measured and expected temperatures T/T_{exp} ; (b) the proton temperature T_p ; (c) the solar wind velocity angles: longitude ϕ and latitude θ ; (d) the z-component of IMF B_z and the y-component of interplanetary electric field E_y ; (e) the measured and density-corrected D_{st} and D_{st}^* indexes; (f) the magnitude of IMF B , the dynamic pressure P_d ; (g) the y- and x-components of IMF (B_y and B_x); (h) the sound and Alfvénic velocities V_s and V_a ; (i) the ion density N , the K_p index increased by coefficient 10; (j) the solar-wind bulk velocity V , the AE index. OMNI dataset has 7h gap for several plasma parameters after IS on 19 December, 1980 but there is total set of IMF measurements.

Both examples show that the magnitude of IMF B has jump at IS from ~ 5 up to $\sim 12 - 15$ nT (factor $\sim 2 - 3$) and then B continues to grow up to ~ 35 nT (total factor ~ 7). In first case the southward component of IMF $|B_z|$ increases up to ~ 30 nT and the compression region Sheath before MC induced the strong magnetic storm with $D_{st} \sim -250$ nT. In second case the southward component $|B_z|$ has two short maxima ~ 17 nT and the compression region Sheath before Ejecta induced the multi-step magnetic storm with $D_{st} \sim -150$ nT. It is important to note that in this case the maximal magnitude of IMF B in Sheath is significantly higher (factor > 2) than in Ejecta.

3.3. Comparison of MC and Ejecta phenomena

Figures 7 and 8 present the temporal profile of 22 SW plasma and IMF parameters for MC (with IS+Sheath, with Sheath and without IS+Sheath - thick, thin and dash red lines, respectively), and Ejecta (with IS+Sheath, with Sheath and without IS+Sheath - thick, thin and dash blue lines) obtained by the double superposed epoch analysis.

1. The bulk velocity V (Fig.7e).

The velocity V decreases for all ICME types and it is higher for phenomena with IS than for phenomena without IS. The velocity differences between subtypes of MC is small and it for subtypes of Ejecta is large: the velocity difference between Ejecta and Ejecta with Sheath is ~ 70 km/s and the velocity difference between Ejecta and Ejecta with Sheath and IS is ~ 100 km/s and these differences are larger at the beginning of interval than at the end.

2. The bulk velocity angles: longitude ϕ and latitude θ (Figs.7c, d).

The angle ϕ decreases from ~ 2 down to ~ 0 degrees for Ejecta with Sheath and IS, from ~ 1 down to ~ 0 degrees for Ejecta with Sheath and without IS and is almost 0 for Ejecta without Sheath. The angle θ is ~ 1 degrees for all subtypes of Ejecta. For MC the angles ϕ and θ have large spread (probably because of small statistics) and a tendency can not be estimated.

3. The density N (Fig.7b).

The density for all types (except MC with Sheath and without IS) has minima in the middle of interval and minimal value ~ 5 cm $^{-3}$ is observed for Ejecta with Sheath and IS. Phenomena with IS have abrupt jumps in the beginning of interval (at the IS front) by

a factor of ~ 5 , other phenomena in the beginning of interval and all phenomena in the end of interval have maxima by a factor of ~ 2 .

4. The proton temperature T_p (Fig.7a).

The temperature for all types decreases in the first half of interval and is almost constant in the second part of interval. Phenomena with IS have jumps in the beginning of interval (at the IS front). The temperature for all subtypes of Ejecta is higher than for similar subtypes of MC.

5. The sound speed V_s (Fig.7g).

The sound speed changes a little throughout the interval, but it is possible to note that it behaves similar to behavior of temperature in the corresponding SW types.

6. The Alfvén speed V_a (Fig.7f).

The Alfvén speed is higher for all subtypes of MC than for Ejecta. It is almost constant for Ejecta and it is lowest for Ejecta without Sheath and IS and highest Ejecta with Sheath and IS (~ 70 km/s). The Alfvén speed has maximum ~ 120 km/s for MC with IS in the middle of interval.

7. The thermal pressure P_t (Fig.7h).

The thermal pressure is closed for phenomena Ejecta and MC, it increases in the ends of interval (there is a jump at the IS front for phenomena with IS).

8. The ratio of measured and expected temperatures T/T_{exp} (Fig.7i).

The ratio of temperatures is closed for phenomena Ejecta and MC, $T/T_{exp} < 1$, and it increases in the ends of interval (there is a jump at the IS front for phenomena with IS).

9. The ratio of proton thermal and magnetic pressures (β -parameter) (Fig.7j).

The ratio is almost constant for all subtypes E and β -parameter ≈ 0.5 . The ratio has minimum ~ 0.1 for MC in the middle of interval.

10. The magnitude of IMF B (Fig.8b).

In accordance with definition of Ejecta and MC, the magnitude of IMF is higher for MC (maximum ~ 15 nT for MC with IS) than for Ejecta (minimum ~ 6 nT for Ejecta without Sheath). For phenomena with IS there is jump at the front of IS and B decreases throughout all interval.

11. The x-, y- and z-components of IMF (B_x , B_y and B_z) (Fig.8c,d,e).

The average values of IMF components is closed to zero for all phenomena, but for MC with IS $B_z < 0$ in the beginning of interval and $B_z > 0$ in the end of interval.

12. The y-component of interplanetary electric field E_y (Fig.8f).

The electric field variation is similar to behavior of IMF B_z component for corresponding SW type.

13. The sound Mach number M_s (Fig.8a).

The sound Mach number decreases for all phenomena throughout all interval. Values M_s is higher for MC than for Ejecta and higher for phenomena with IS than for phenomena without IS.

14. The Alfvén Mach number M_a (Fig.8g).

The Alfvén Mach number is low for all phenomena. Values M_a is higher for Ejecta than for MC and lower for phenomena with IS than for phenomena without IS.

15. The dynamic pressure P_d (Fig.8h).

The dynamic pressure is almost constant for all phenomena (phenomena with IS have a jump in the beginning of interval) and it is higher for MC than for Ejecta.

16. The magnetospheric AE , K_p , D_{st} and D_{st}^* indices (Fig.8i,j,k,l).

All indices show that magnetospheric activity decreases throughout all interval. The activity is higher for MC than for Ejecta and for phenomena with IS than phenomena without IS.

4. Discussion and Conclusions

As has been noted in our first article [Yermolaev et al., 2015], in general, our results on compression regions are close to earlier published data (e.g. Jian et al. [2008]; Borovsky and Denton [2010]; Mitsakou and Moussas [2014] and references therein), but unlike the previous works we carried out additional selection of events by types of pistons and existence of IS. In the present work we compare several key parameters in more detail taking into account this selection. For the majority of parameters their behavior is close for different pistons, but depends on the existence of IS. For example, all types of compression regions have on average identical speed profiles both in value and in inclination, and the increase of speed of pistons on 100 km/s leads to formation of IS. For some parameters the main difference consists in their jump at the beginning of interval.

Obtained data allows us to suggest that the formation of all types of compression regions has the same physical mechanism irrespective of piston type. To check this hypothesis, it would be useful to compare not only full jumps of speed in compression regions (see figure 1e), but also speed gradients in these regions. It should be noted that the presented average temporary profiles of speed do not allow one to directly define the average gradients of speed for various types of compression regions as measurements are carried out under unknown angle relative to the speed gradient. If making the natural assumption that the gradient of speed is directed approximately on normals to the piston, CIR has

the greatest angle between the gradient of speed and the direction of average SW speed, and ICME - the smallest angle (in order that the satellite can cross ICME body, it has to be near a nose area of ICME). The average real (before the rescaling during DSEA processing) durations of compression regions considerably differ: for figures 1 and 2 we took duration of CIR of 20 hours (close to real), and the average real durations of Sheath before Ejecta and Sheath before MC are shorter by a factor of ~ 1.5 and ~ 2 , respectively (e.g. *Yermolaev et al.* [2010b]). This duration difference is qualitatively agree with the assumption that all types of compression regions have approximately identical sizes in the direction of speed gradient, and taking into account the identical total jumps of speed in compression regions (see figure 1e) they have also identical gradients of speed. One of consequences of this hypothesis is the conclusion that one of the reasons of observed distinctions of parameters in MC and Ejecta can be fact that at measurements of Ejecta the satellite passes further from the nose area of ICME, than at measurements of MC, i.e. distinctions can be connected partially with conditions of observation, but not with physical distinctions between Ejecta and MC. This result agrees with geometrical selection of ICME measurements described by *Jian et al.* [2006].

Increase of piston speed increases the magnitude of magnetic field and its components in the compression regions and, as a result, magnetospheric disturbances. As show the presented results the IMF magnitude can reach rather high value, and ratios of average and maximum values to level of undisturbed SW can be > 4 in 1.5 and 6% of cases, respectively. This percentage of events is close to percentage of strong magnetic storms [?]. At average dependences of B on piston speed (see figures 3 and 4) the SW speeds observed in experiments can lead to great values of IMF field. So at a speed in HSS more

than 1000 km/s the magnetic field in CIR can increase to 50–70 nT, and at a speed of MC \sim 2000 km/s (as, for example, in events of August of 1972 [*Vaisberg and Zastenker, 1976*]) up to 100 nT. It should be note that efficiency of magnetic storm generation is \sim 50% higher for Sheath and CIR than for ICME (MC and Ejecta) [*Nikolaeva et al., 2013, 2015*], i.e. at identical southward components of interplanetary field the magnetic storms are generated \sim 1.5 times more strongly by Sheath and CIR than by ICME. Thus it is possible to conclude that in our opinion the role of compression regions (especially Sheath) in generation of storms is often underestimated.

On the other hand, the wrong estimation of contribution of Sheath magnetic field in the IMF can lead to mistakes in studying of magnetic field of the Sun. Several recent works proposed that the Sun’s open magnetic field flux consists of a time-independent (floor) component which may be observed during solar minimum and a time-varying component due to CMEs (see recent papers by *Wang and Sheeley [2015]*; *Cliver and von Steiger [2015]* and references therein). Because the Sheaths originate from outside the CMEs in the Sun, the inclusion of the Sheaths in the ICMEs (see, for example, catalog by ?) can result in significant overestimation of the contribution of the CME itself to the IMF and incorrect estimation of Sun’s open magnetic flux on the basis of interplanetary measurements [*Yermolaev et al., 2009b*].

It would be desirable to pay attention of the reader to the interesting fact: at the analysis of all events (without selection by their geoefficiency) the magnetosphere activity for CIR/Sheath increases in interval but for MC/Ejecta it increases in the beginning of interval and then decreases.

Figures 7 and 8 show that all ICME types have several traces of compression near interval edges (more strongly on the leading edge and more weakly on the training edge): (1) the increase of density n , (2) the of temperatures T_p and T_p/T_{exp} , (3) the increase of dynamic and thermal pressures P_d and P_k , (4) the increase of β -parameter, and (5) the turn of speed angle ϕ . These facts confirm the ICME expansion and its interaction with surrounding solar wind. As the average velocity of ICME is higher than that of surrounding solar wind, the compression on the leading edge is higher than on the training edge.

Acknowledgments. The authors are grateful for the opportunity to use the OMNI database. The OMNI data were obtained from GSFC/ SPDF OMNIWeb (<http://omniweb.gsfc.nasa.gov>). YY is grateful to SCOSTEP's "Variability of the Sun and Its Terrestrial Impact" (VarSITI) program for the support of his participation in the workshop "International Study for Earth-Affecting Solar Transients (ISEST)/MiniMax" in Mexico City, Mexico, October 26 – 30, 2015. This work was supported by the Russian Foundation for Basic Research, project 16-02-00125, and by Program 7 of Presidium of the Russian Academy of Sciences.

References

- Akasofu, S.-I. (1981), Energy coupling between the solar wind and the magnetosphere, *Space Sci. Rev.*, 111, A07S08, doi:10.1029/2005JA011447.
- Bendat, J. S. and Piersol, A. G., (1971) *Measurement and Analysis of Random Data*, Wiley-Interscience.

- Borovsky, J. E., and M. H. Denton (2010), Solar wind turbulence and shear: A superposed-epoch analysis of corotating interaction regions at 1 AU, *J. Geophys. Res.*, 115, A10101, doi:10.1029/2009JA014966.
- Burton, R. K., McPherron, R. L., and Russell, C. T (1975), An empirical relationship between interplanetary conditions and Dst, *J. Geophys. Res.*, 80, 4204–4214.
- Cid, C., J., Palacios, E. Saiz, A. Guerrero, and Y. Cerrato (2014), On extreme geomagnetic storms *J. Space Weather Space Clim.* 4 A28 DOI: 10.1051/swsc/2014026
- Cliver, E. W.; R. von Steiger (2015), Minimal Magnetic States of the Sun and the Solar Wind: Implications for the Origin of the Slow Solar Wind , *Space Science Reviews*, DOI: 10.1007/s11214-015-0224-1
- Gonzalez, W. D., Tsurutani, B. T., and Clua de Gonzalez, A. L. (1999), Interplanetary origin of geomagnetic storms, *Space Sci. Rev.*, 88, 529–562.
- Gopalswamy, N., Tsurutani, B., and Yan, Y. (2015) Short-term variability of the Sun-Earth system: an overview of progress made during the CAWSES-II period, *Progress in Earth and Planetary Science*, 2, 13 DOI 10.1186/s40645-015-0043-8
- Gopalswamy, N., S. Yashiro, H. Xie, S. Akiyama, and P. Makela (2015), Properties and geoeffectiveness of magnetic clouds during solar cycles 23 and 24, *J. Geophys. Res. Space Physics*, 120, 9221?9245, doi:10.1002/ 2015JA021446.
- Hietala, H., E. K. J. Kilpua, D. L. Turner, and V. Angelopoulos (2014), Depleting effects of ICME-driven sheath regions on the outer electron radiation belt, *Geophys. Res. Lett.*, 41, 2258?2265, doi:10.1002/2014GL059551.
- Huttunen, K. E. J. and Koskinen, H. E. J. (2004), Importance of postshock streams and sheath region as drivers of intense magnetospheric storms and high-latitude activity,

Ann. Geophys., 22, 1729–1738, doi:10.5194/angeo-22-1729-2004.

Jian, L. K., C. T. Russell, J. G. Luhmann, R. M. Skoug, (2006) Properties of interplanetary coronal mass ejections at one AU during 1995–2004, *Solar Physics*, 239, pp. 393–436

Jian, L. K., C. T. Russell, J. G. Luhmann, R. M. Skoug, and J. T. Steinberg (2008), Stream Interactions and Interplanetary Coronal Mass Ejections at 0.72 AU, *Solar Phys*, v. 249, pp. 85–101 DOI 10.1007/s11207-008-9161-4

Katus, R. M., M. W. Liemohn, E. L. Ionides, R. Ilie, D. Welling, and L. K. Sarnoff-Smith (2015), Statistical analysis of the geomagnetic response to different solar wind drivers and the dependence on storm intensity, *J. Geophys. Res. Space Physics*, 120, doi:10.1002/2014JA020712.

King, J.H. and Papitashvili, N.E., (2004), Solar Wind Spatial Scales in and Comparisons of Hourly Wind and ACE Plasma and Magnetic Field Data, *J. Geophys. Res.*, vol. 110, no. A2, p. A02209. doi: 10.1029/2004JA010804.

Kilpua, E. K. J., H. Hietala, D. L. Turner, H. E. J. Koskinen, T. I. Pulkkinen, J. V. Rodriguez, G. D. Reeves, S. G. Claudepierre, and H. E. Spence (2015), Unraveling the drivers of the storm time radiation belt response. *Geophys. Res. Lett.*, 42, 3076–3084. doi: 10.1002/2015GL063542.

Mitsakou, E., and X. Moussas (2014), Statistical Study of ICMEs and Their Sheaths During Solar Cycle 23 (1996 – 2008), *Solar Phys* 289:3137–3157 DOI 10.1007/s11207-014-0505-y

Nikolaeva, N. S., Yu. I. Yermolaev, and I. G. Lodkina, (2013), Modeling of Dst-index temporal profile on the main phase of the magnetic storms generated by different types

- of solar wind, *Cosmic Research*, 2013, Vol. 51, No. 6, pp. 401–412 (Kosmicheskie Issledovaniya, 2013, v. 51, N 6, pp. 443–454)
- Nikolaeva, N. S., Yu. I. Yermolaev, and I. G. Lodkina, (2015), Modeling of the Corrected *Dst** Index Temporal Profile on the Main Phase of the Magnetic Storms Generated by Different Types of Solar Wind, *Cosmic Research*, 2015, Vol. 53, No. 2, pp. 119–127. (Kosmicheskie Issledovaniya, 2015, Vol. 53, No. 2, pp. 126–135.
- Richardson, I. G., H.V. Cane (2012), Near-earth solar wind flows and related geomagnetic activity during more than four solar cycles (1963–2011), *J. Space Weather Space Clim.* 2 A02 DOI: 10.1051/swsc/2012003
- Russell, C. T., McPherron, R. L., and Burton, R. K., (1974), On the cause of magnetic storms, *J. Geophys. Res.*, 79, 1105–1109.
- Thatcher, L. J., and H.-R. Müller (2011), Statistical investigation of hourly OMNI solar wind data, *J. Geophys. Res.*, 116, A12107, doi:10.1029/2011JA017027.
- Tsurutani, B. T., Gonzalez, W. D., Gonzalez, A. L. C., Guarnieri, F. L., Gopalswamy, N., Grande, M., Kamide, Y., Kasahara, Y., Lu, G., Mann, I., McPherron, R., Soraas, F., and Vasyliunas, V. (2006), Corotating solar wind streams and recurrent geomagnetic activity: A review, *J. Geophys. Res.*, 111, A07S01, doi:10.1029/2005JA011273,
- Vaisberg, O. L., Zastenker, G. N. (1976) Solar wind and magnetosheath observations at Earth during August 1972, *Space Science Reviews*, Volume 19, Issue 4, pp 687-702
- Wang, Y.-M.; Sheeley, N. R., Jr. (2015) Coronal Mass Ejections and the Solar Cycle Variation of the Sun's Open Flux *The Astrophysical Journal Letters*, Volume 809, Issue 2, article id. L24 DOI: 10.1088/2041-8205/809/2/L24

Wimmer-Schweingruber, R. F., Crooker, N. U., Balogh, A., Bothmer, V., Forsyth, R. J., Gazis, P., Gosling, J. T., Horbury, T., Kilchenmann, A., Richardson, I. G., Richardson, J. D., Riley, P., Rodriguez, L., Von Steiger, R., Wurz, P., and Zurbuchen, T. H. (2006) Understanding Interplanetary Coronal Mass Ejection Signatures, *Space Sci. Rev.*, 123(1?3), 177?216.

Wu, C.-C., and R. P. Lepping (2015), Comparisons of Characteristics of Magnetic Clouds and Cloud-Like Structures During 1995 ? 2012 *Solar Phys*, DOI 10.1007/s11207-015-0656-5

Yermolaev, Yu. I. and M. Yu. Yermolaev, (2006), Statistic Study on the Geomagnetic Storm Effectiveness of Solar and Interplanetary Events, *Adv. Space Res.* 37(6), 1175–1181.

Yermolaev, Yu.I., and M.Yu. Yermolaev, (2010), Solar and Interplanetary Sources of Geomagnetic Storms: Space Weather Aspects, *Izvestiya, Atmospheric and Oceanic Physics*, 46(7), 799–819.

Yermolaev, Yu. I., Yermolaev, M. Yu., Nikolaeva, N. S., and Lodkina, L. G. (2007), Interplanetary conditions for CIR-induced and MC induced geomagnetic storms, *Bulg. J. Phys.*, 34, 128–135.

Yermolaev, Yu. I., et al., (2009), Catalog of Large-Scale Solar Wind Phenomena during 1976–2000, *Kosm. Issled.*, vol. 47, no. 2, pp. 99–113. [Cosmic Research, pp. 81–94].

Yermolaev, Y. I.; Lodkina, I. G.; Nikolaeva, N. S.; Yermolaev, M. Y. (2009) The “Floor” in the Interplanetary Magnetic Field: Estimation on the Basis of Relative Duration of ICME Observations in Solar Wind During 1976 - 2000, *Solar Physics*, Volume 260, Issue 1, pp.219-224

- Yermolaev, Yu. I., N. S. Nikolaeva, I. G. Lodkina, and M. Yu. Yermolaev, (2010), Specific interplanetary conditions for CIR-, Sheath-, and ICME-induced geomagnetic storms obtained by double superposed epoch analysis, *Ann. Geophys.*, *28*, 2177–2186.
- Yermolaev, Yu. I., N. S. Nikolaeva, I. G. Lodkina, and M. Yu. Yermolaev, (2010), Large-scale solar wind structures: occurrence rate and geoeffectiveness, TWELFTH INTERNATIONAL SOLAR WIND CONFERENCE. AIP Conference Proceedings, Volume 1216, pp. 648-651
- Yermolaev, Y. I., N. S. Nikolaeva, I. G. Lodkina, and M. Y. Yermolaev (2012), Geoeffectiveness and efficiency of CIR, sheath, and ICME in generation of magnetic storms, *J. Geophys. Res.*, *117*, A00L07, doi:10.1029/2011JA017139
- Yermolaev, Yu. I., I. G. Lodkina, N. S. Nikolaeva, and M. Yu. Yermolaev (2015), Dynamics of large-scale solar wind streams obtained by the double superposed epoch analysis, *J. Geophys. Res. Space Physics*, *120*, doi:10.1002/2015JA021274
- Zhang, J., Richardson, I. G., Webb, D. F., Gopalswamy, N., Huttunen, E., Kasper, J. C., Nitta, N. V., Poomvises, W., Thompson, B. J., Wu, C.-C., Yashiro, S., and Zhukov, A. N. (2007), Solar and interplanetary sources of major geomagnetic storms ($Dst < -100$ nT) during 1996–2005, *J. Geophys. Res.*, *112*, A10102, doi:10.1029/2007JA012321.
- Zurbuchen, T. H., and I. G. Richardson (2006), In-Situ Solar Wind and Magnetic Field Signatures of Interplanetary Coronal Mass Ejections, *Space Science Reviews*, V. 123, N. 1-3, pp 31-43

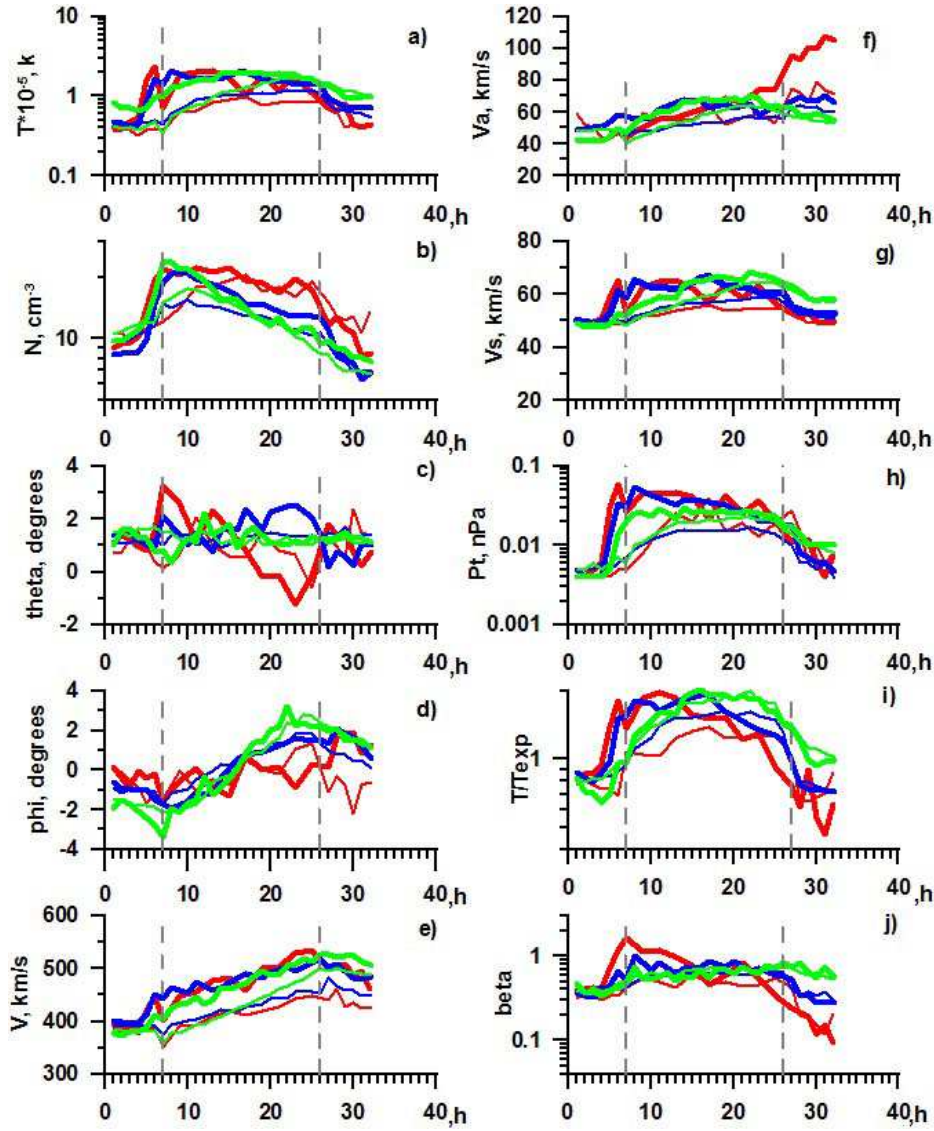


Figure 1. The temporal profile of SW plasma and IMF parameters for CIR (with IS and without IS - bold and thin green lines, respectively) and Sheath before Ejecta (with IS and without IS - bold and thin blue lines) and Sheath before MC (with IS and without IS - bold and thin red lines) obtained by the double superposed epoch analysis

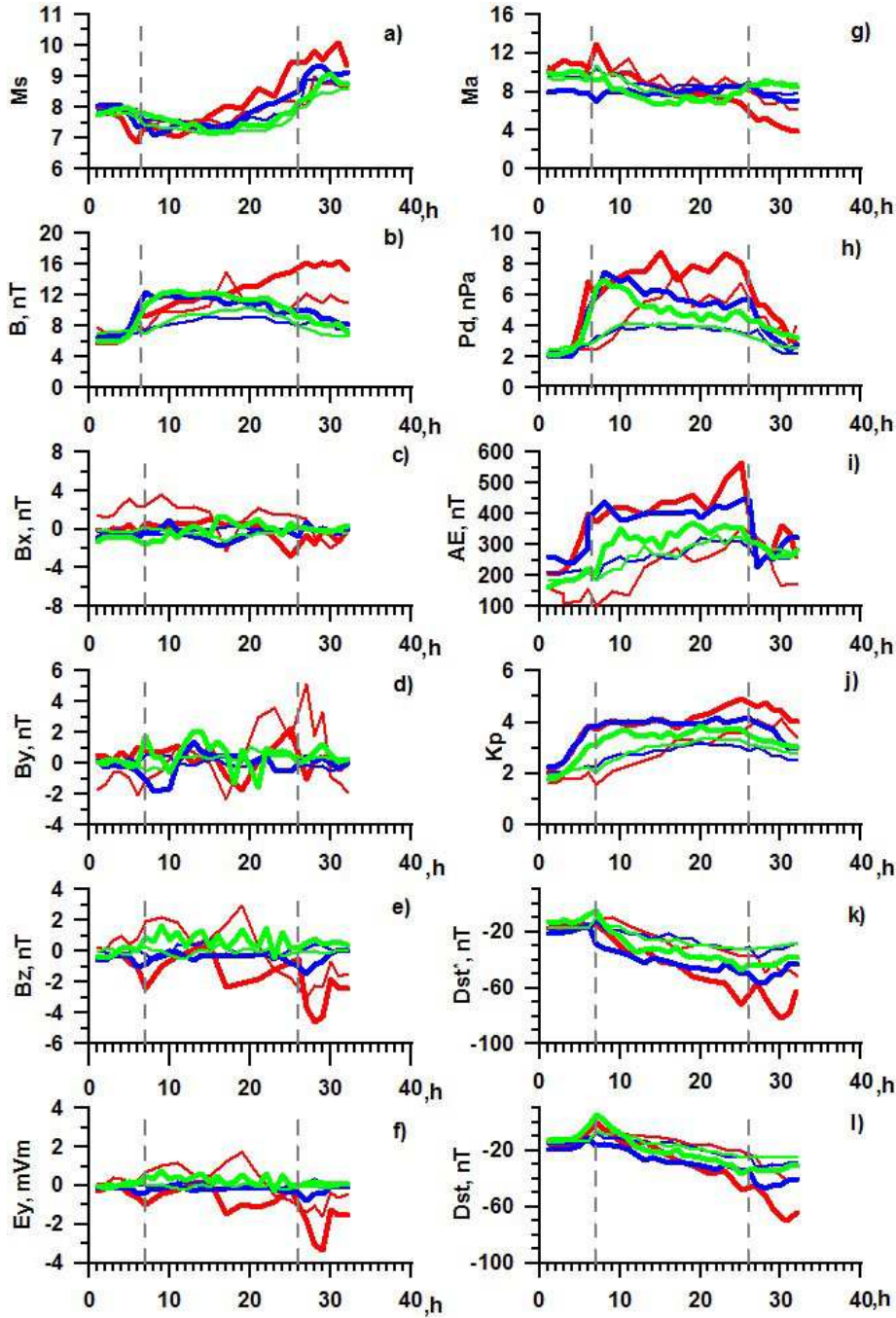


Figure 2. Continuation of figure 1

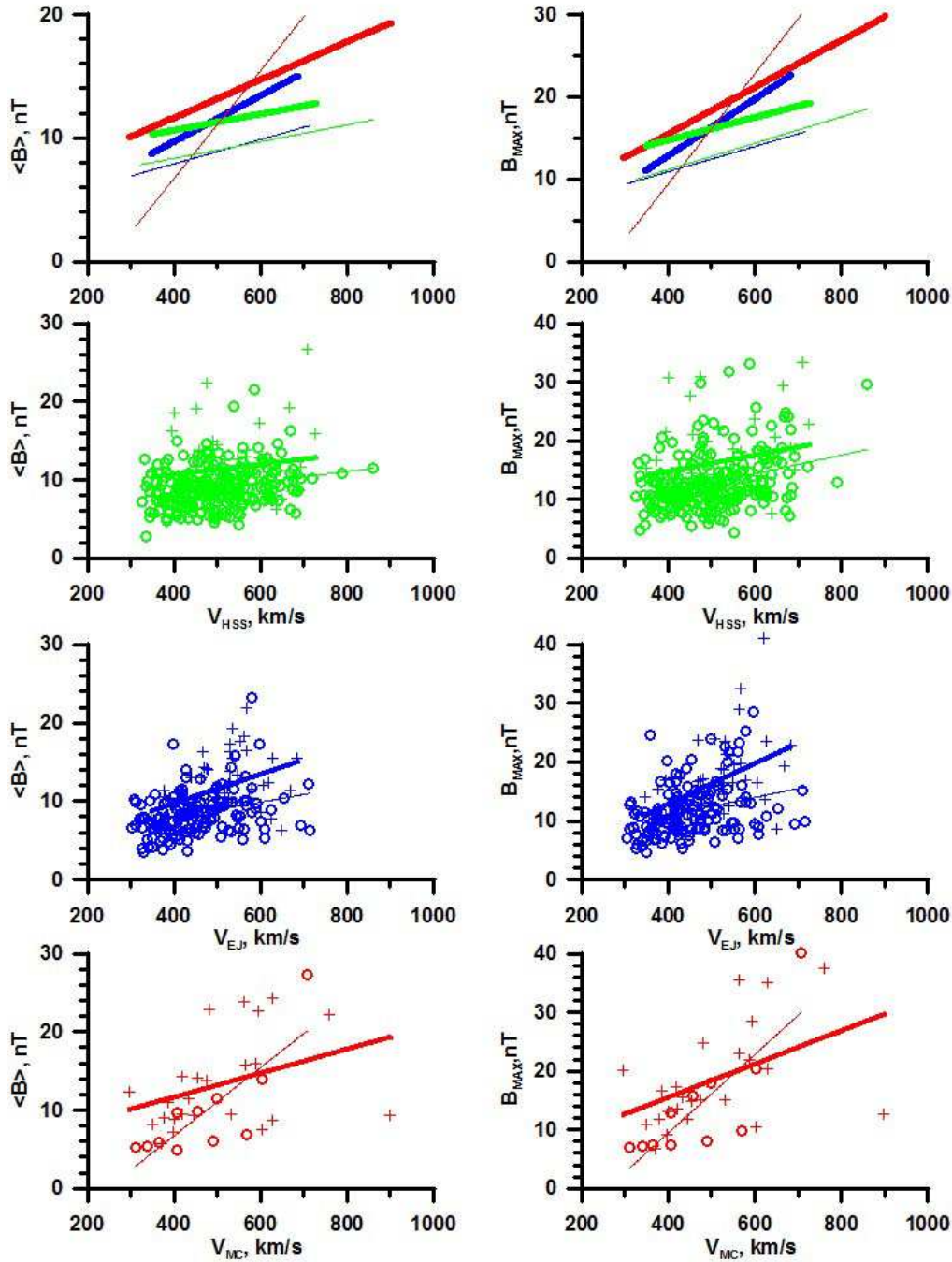


Figure 3. Dependence of the average and maximal values of magnetic field $\langle B \rangle$ and B_{max} on the speed of piston for CIR (green), Sheath before Ejecta (blue) and Sheath before MC (red). Bold lines and circles for events with IS, thin lines and crosses for events without IS

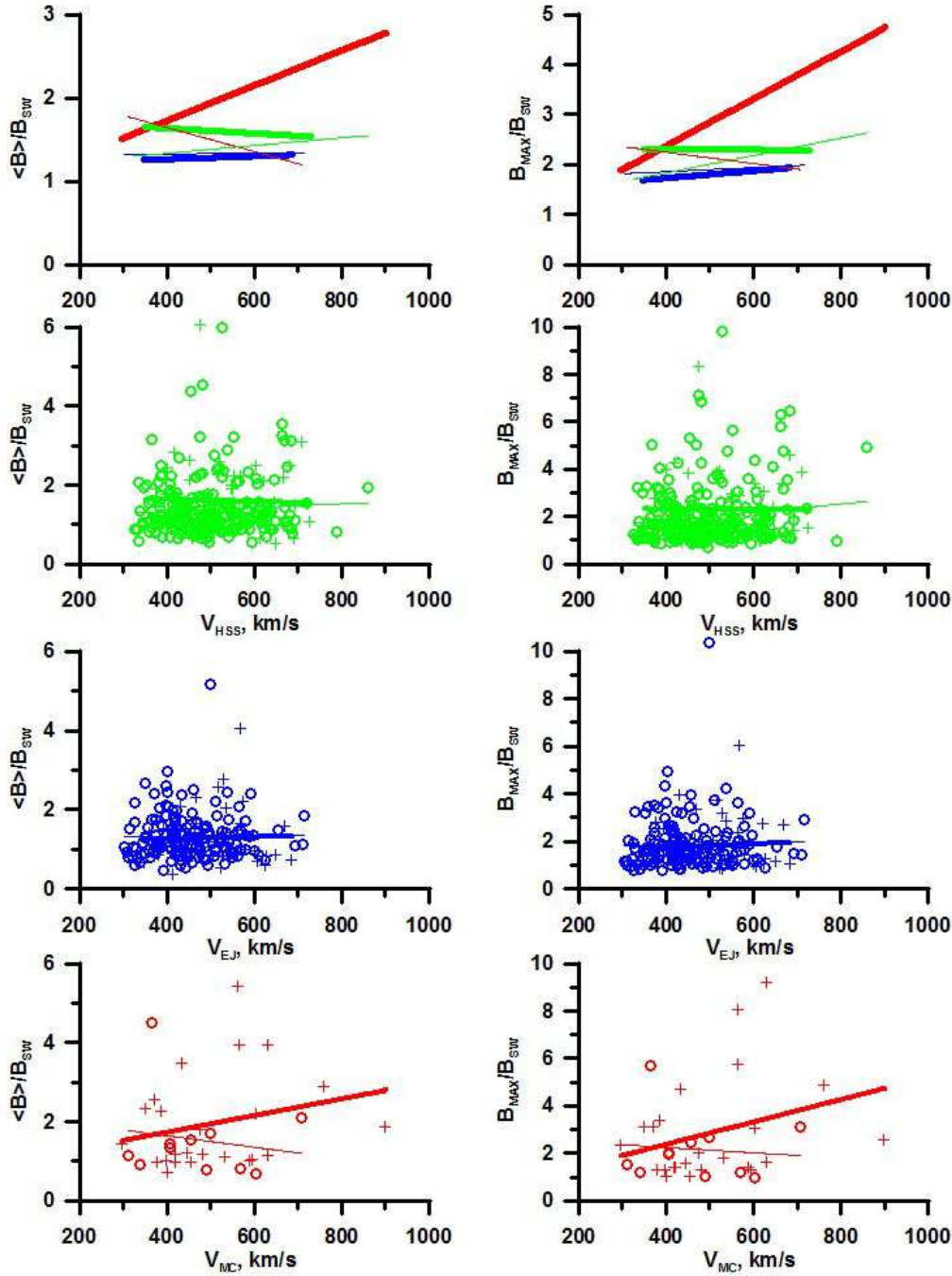


Figure 4. The same dependence of normalized values $\langle B \rangle / B_{SW}$ and B_{max} / B_{SW}

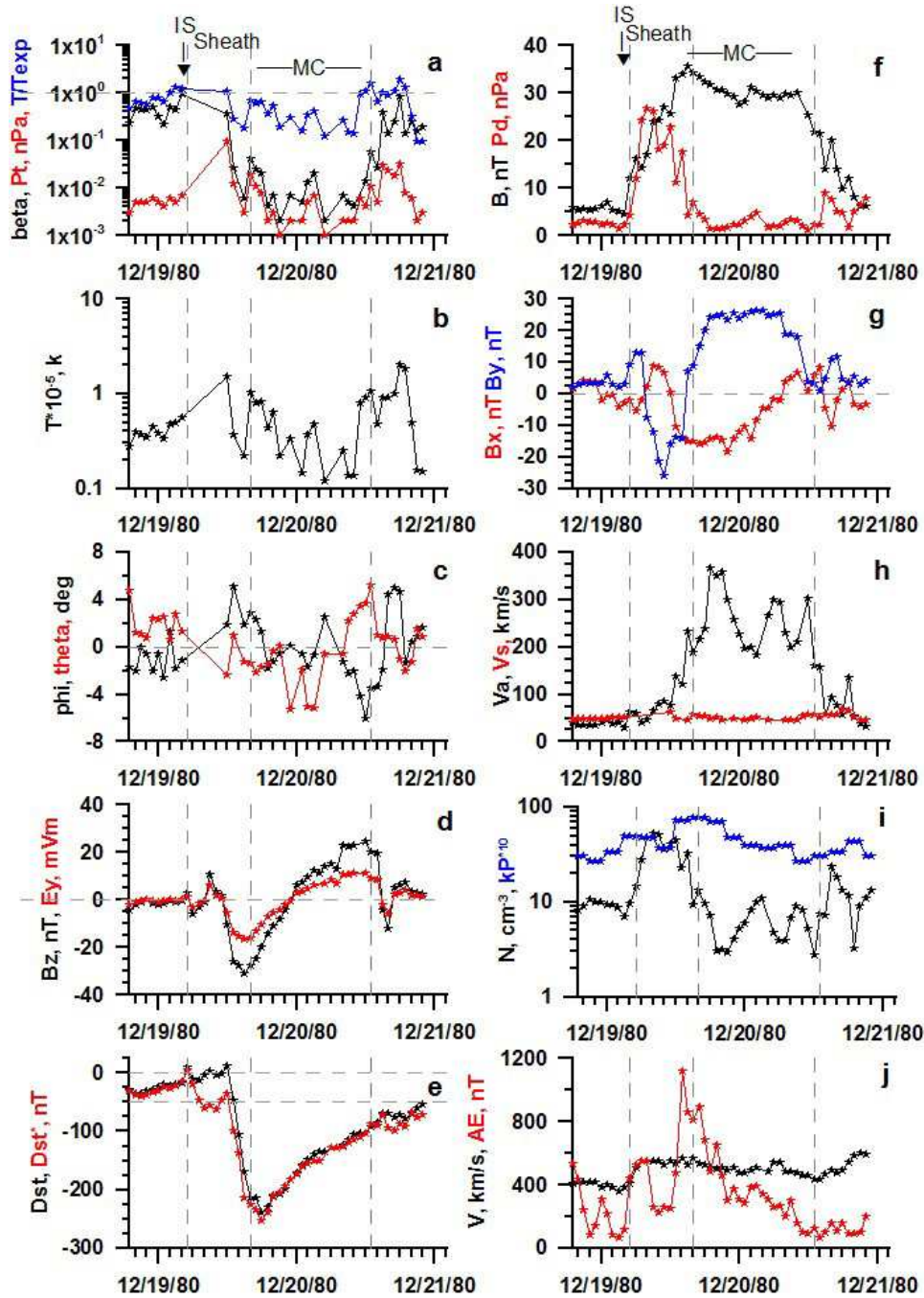


Figure 5. The temporal profile of SW plasma and IMF parameters for consequence SW/IS/Sheath/MC/SW in period of 18-21 December 1980

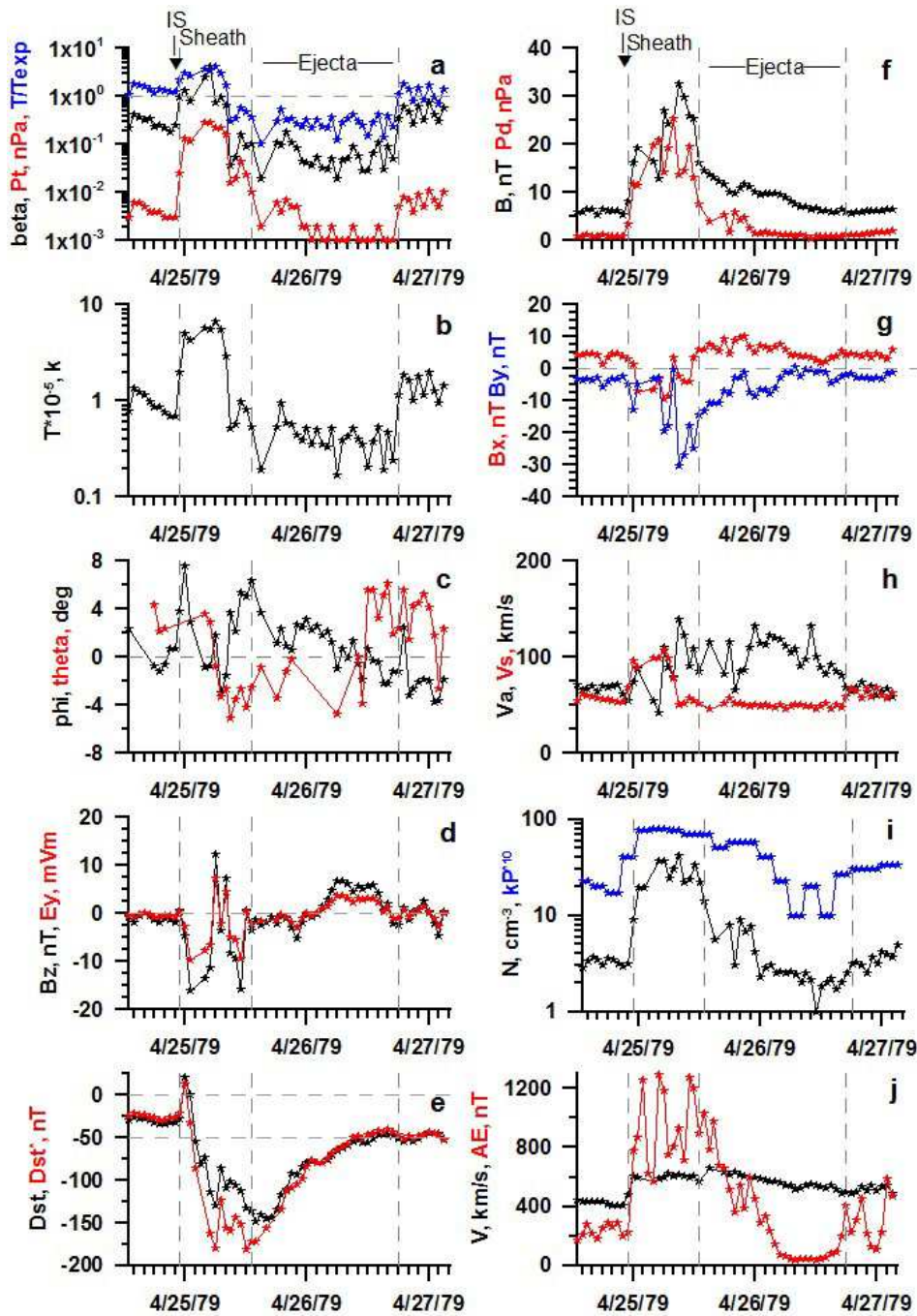


Figure 6. The temporal profile of SW plasma and IMF parameters for SW/IS/Sheath/Ejecta/SW in period of 24-27 April 1979

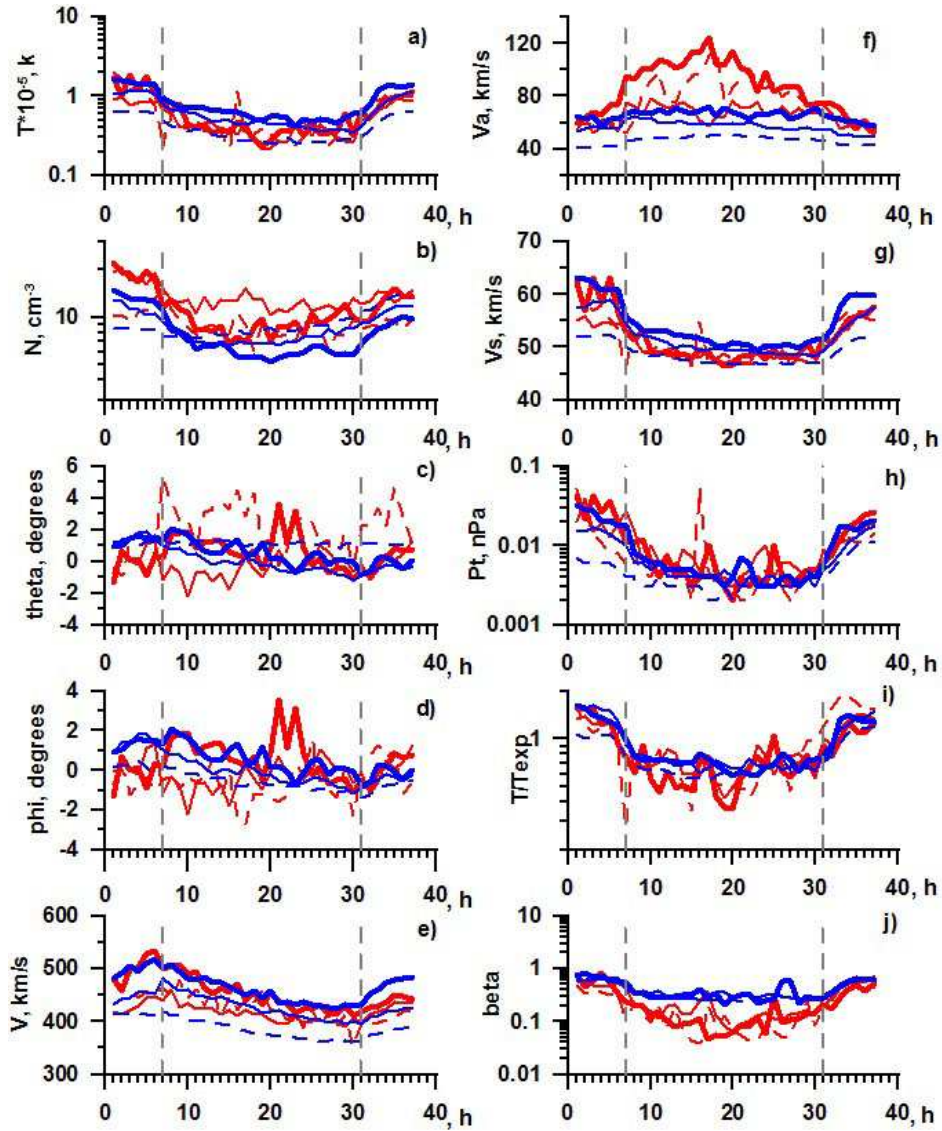


Figure 7. The temporal profile of SW plasma and IMF parameters for MC (with IS+Sheath, with Sheath and without IS+Sheath - bold, thin and dash red lines, respectively), and Ejecta (with IS+Sheath, with Sheath and without IS+Sheath - bold, thin and dash blue lines) obtained by the double superposed epoch analysis

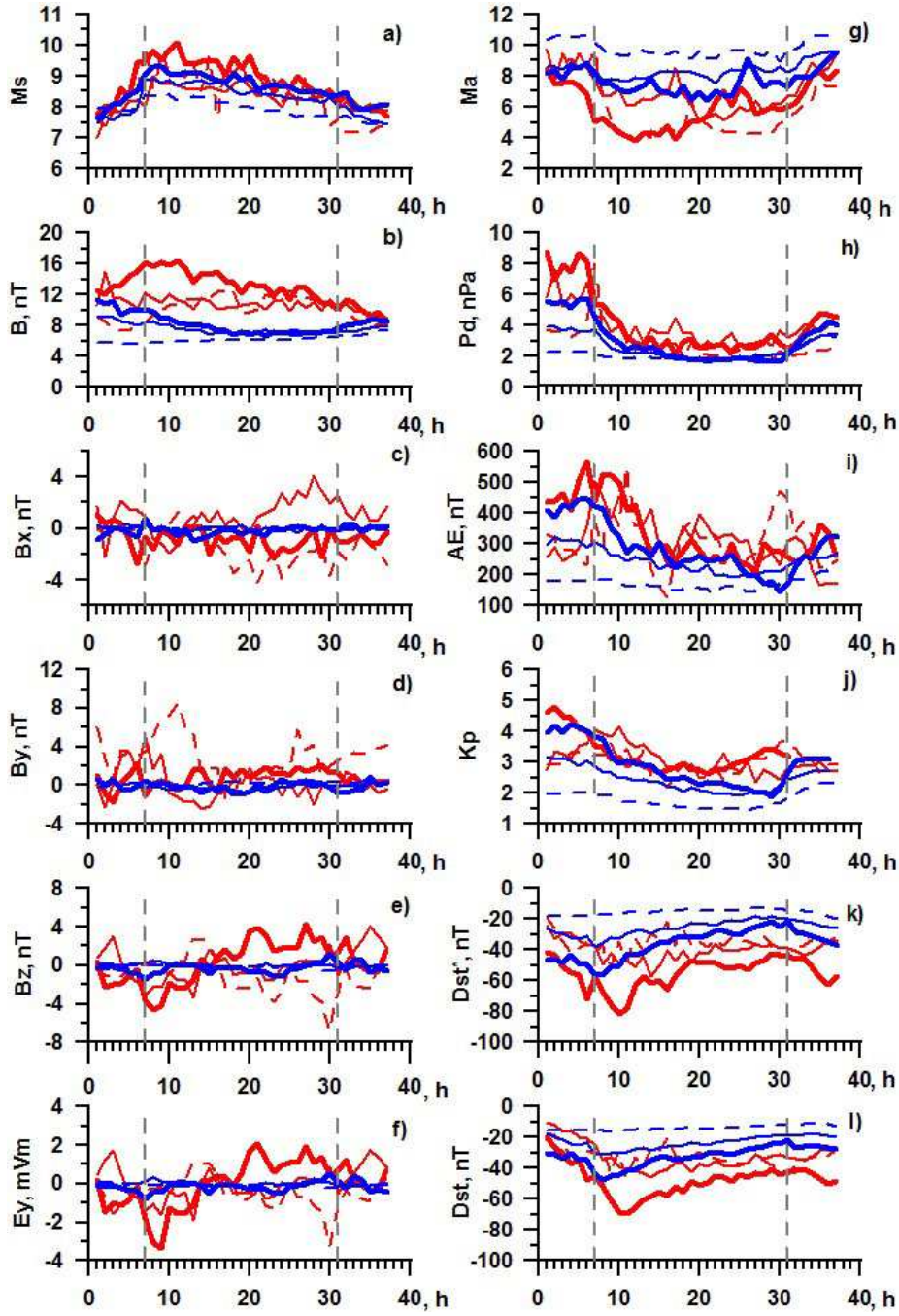


Figure 8. Continuation of figure 7